

Nonstandard electroconvection and flexoelectricity in nematic liquid crystals

Alexei Krekhov* and Werner Pesch

Physikalisches Institut, Universität Bayreuth, D-95440 Bayreuth, Germany

Nándor Éber, Tibor Tóth-Katona, and Ágnes Buka

*Research Institute for Solid State Physics and Optics,
Hungarian Academy of Sciences, H-1525 Budapest, P.O.B.49, Hungary*

(Dated: September 3, 2007)

For many years it has been commonly accepted that electroconvection (EC) as primary instability in nematic liquid crystals for the “classical” planar geometry requires a positive anisotropy of the electric conductivity, σ_a , and a slightly negative dielectric anisotropy, ϵ_a . This firm belief was supported by many experimental and theoretical studies. Recent experiments, which have surprisingly revealed EC patterns at negative conduction anisotropy as well, have motivated the new theoretical studies in this paper. It will be demonstrated that including the usually neglected flexoelectric effect into the standard EC model provides a natural explanation for EC in the “nonstandard” case $\sigma_a < 0$. The theoretical results and the experiments match well.

PACS numbers: 61.30.Gd, 47.54.-r, 64.70.Md

I. INTRODUCTION

In the last decades electroconvection (EC) in nematic liquid crystals (nematics) has developed into an attractive model system to study generic aspects of pattern-forming non-equilibrium phase transitions in extended systems [1, 2]. Nematics are anisotropic liquids without translational but with long-range uniaxial orientational order of their elongated molecules, which is described by the director field \mathbf{n} [3, 4]. EC occurs when an electric voltage above a critical threshold is applied to a layer of a nematic, which is sandwiched between two supporting transparent electrodes of distance d (typically $5 \mu\text{m} < d < 50 \mu\text{m}$). At onset usually periodic arrays of stripes with wave vector \mathbf{q} are observed. The patterns are associated with periodic spatial modulations in the director and the flow field (“convection rolls”) and also in the charge and current density. Due to the intrinsic uniaxial anisotropy of nematics EC is more diverse than for instance the canonical, thermally driven, isotropic Rayleigh-Bénard convection. It is also an experimentally convenient system: the patterns are easy to visualize by exploiting the birefringence of nematics and contain usually many well ordered convection rolls. The main control parameters (amplitude and frequency of the applied voltage) can be varied over a wide range.

In the standard theoretical description of EC (the *standard model*) the fluid flow, \mathbf{v} , is described by the Navier-Stokes equations, coupled to the Maxwell equations for the electric properties [1–6]. The director dynamics is governed by elastic, electric and viscous torques. The main ingredients of EC have been elucidated by Carr [7] and Helfrich [8]: any spatial director fluctuation leads to a finite charge density, ρ_{el} , and consequently in the pres-

ence of electric fields to Coulomb forces and thus to flow (mass transport). If the resulting viscous torques reinforce the initial director fluctuation the EC instability is triggered.

Whether the positive feedback loop leading to EC is really excited depends first on the material parameters and their anisotropies. Most of them (e.g., elastic constants, viscosities) do not change significantly from substance to substance; thus they are not decisive. The key quantities are the dielectric and the conductivity anisotropies, which may considerably vary in their magnitude and may even change sign. Furthermore the initial director alignment in the nematic layer which is imposed by a suitable surface treatment of the confining electrodes plays an important role. A recent comprehensive overview of the EC onset behavior considering all these aspects is given in [9].

In this paper we concentrate on the mostly studied *planar* configuration, where the director in the basic state, \mathbf{n}_0 , is oriented in a direction parallel to the confining plates (our x -axis). According to the standard model EC requires in this case a positive anisotropy of the electric conductivity $\sigma_a = \sigma_{\parallel} - \sigma_{\perp}$, where σ_{\parallel} and σ_{\perp} denote the conductivities parallel and perpendicular to the director, respectively. Furthermore the dielectric anisotropy $\epsilon_a = \epsilon_{\parallel} - \epsilon_{\perp}$ has to be negative or only slightly positive. Theory is in excellent agreement with numerous experiments on various nematic compounds (see, e.g., [1, 10] and references therein).

Electroconvection in the familiar case of an applied voltage with frequency f is a parametrically driven system; consequently \mathbf{n} and \mathbf{v} oscillate in time as well. It turns out, that in general, depending on f , two different solution types of the basic equations can be identified: at low f below the crossover frequency, f_c , in the “conductive regime” the time average of the induced charge density is practically zero, while the time averages of the other fields (director, flow) are finite. In the high-frequency “dielectric regime” ($f > f_c$) the situation is

*alexei.krekhov@uni-bayreuth.de

reversed.

Our motivation to reconsider EC from a theoretical point of view stems from experiments in the planar geometry carried out on some members of the 4-n-alkoxyphenyl-4-n'-alkoxybenzoates homologous series [11] of nematic materials. They are characterized by $\epsilon_a < 0$ and $\sigma_a < 0$ in the lower temperature range of the nematic (N) phase. At the higher temperature end of the N phase, however, they possess $\sigma_a > 0$ as common for nematics, i.e., $\sigma_a(T)$ changes sign in between as function of temperature T . First experiments on these substances have indeed revealed the expected extended EC roll patterns for the temperature range where $\sigma_a(T) > 0$ [12]. In the regime $\sigma_a(T) < 0$, where the standard model does not predict any convection instability, a new kind of a localized structure has been described, which has reminded to the “worms” discussed in [13]. These experiments have been recently repeated more systematically [14, 15] and the main features of the patterns described in [12] have been reproduced for the temperature range where $\sigma_a(T) > 0$. Surprisingly, however, when $\sigma_a(T) < 0$ extended roll patterns have been found as well. This phenomenon, which is not explained by the standard model, has been coined as *nonstandard* EC (ns-EC).

The ns-EC patterns have been found to differ significantly from the standard ones [2, 15]. A most salient feature of ns-EC rolls is the angle, α , between \mathbf{n}_0 and the wave vector \mathbf{q} . While α is typically zero or at least small ($< 30^\circ$, say) in standard EC, it is large ($> 60^\circ$) in ns-EC and approaches even 90° in some cases.

Instead of speculating about some new, fancy EC mechanism we found it reasonable to reconsider the standard theoretical treatment of EC, but with special emphasis on topics not completely analyzed before. In view of the importance of the charge separation within the Helfrich mechanism, it has been suggestive to focus on the so called *flexoelectric* (shortened to *flexo* in the following) *polarization* [3, 4, 16]. It appears in the presence of director distortions even in the absence of an external electric field and produces an additional contribution to ρ_{el} . An additional motivation to consider in more detail the flexo effect was the unusual roll orientation mentioned before. In fact, it has been described already many years ago [17, 18], that the flexo effect produces a torque on the director in the presence of a dc voltage, which may lead to striped (though non-convective) patterns with the extreme roll orientation $\alpha = 90^\circ$.

Earlier investigations of the flexo polarization in standard EC with $\sigma_a > 0$ have basically focused on the low frequency (conductive) regime [19, 20] and have led to the general impression that the flexo polarization plays a minor role, since only small quantitative changes of the critical voltage and the critical wave vector have been reported. Consequently the flexo mechanism has typically been neglected in the theoretical analysis of EC. Moreover, the two additional material parameters, the flexo coefficients e_1 and e_3 , which come into play are not easy to measure. In contrast, it will be demonstrated in this

paper, that the flexo polarization plays a crucial role in the nonstandard case when $\sigma_a < 0$ and $\epsilon_a < 0$. It allows in fact for the EC instability, which was excluded in the standard model for this parameter combination.

The paper is organized as follows. Sect. II is devoted to the implementation of the linear stability analysis of the basic state, which is characterized by the uniform planar director configuration \mathbf{n}_0 in the absence of material flow and electrical space charge. From the nematohydrodynamic equations one arrives at a linear eigenvalue problem for the growth rate of perturbations in form of convection rolls, from which we obtain the critical data at onset. We focus in particular on the flexo effect and exploit certain spatial and temporal invariance properties of the linear equations to classify the patterns with respect to their symmetries. In Sect. III we present and discuss the results of the linear analysis, i.e., the critical voltage and the critical wave vector. Instead of extended parameter studies we focus on the qualitative features of the positive feedback loop leading to EC and especially on the σ_a dependence. We also compare the theoretical results with experiments. In Sect. IV we draw some conclusions. In the Appendix we present explicitly the formulation of the linear eigenvalue problem discussed in this paper, also in order to introduce the notation.

II. LINEAR STABILITY ANALYSIS

The behavior of nematic liquid crystals in the framework of the standard model is covered by standard nematohydrodynamics (see, e.g., [3–6]). In this paper we are only interested in the onset behavior of EC to obtain the critical voltage and the critical wave vector. Their determination requires an analysis of the nematohydrodynamic equations linearized about the basic state. They are presented in the Appendix and can be found already in [6] except the flexo-terms $\propto e_1, e_3$.

Let us consider in more detail the flexo polarization \mathbf{P}_{fl} , which appears at first in the Maxwell equations within the quasi-static approximation, where ρ_{el} is obtained from charge conservation and Poisson’s law:

$$\frac{\partial \rho_{el}}{\partial t} + \nabla \cdot (\boldsymbol{\sigma} \mathbf{E} + \rho_{el} \mathbf{v}) = 0, \quad \rho_{el} = \nabla \cdot \mathbf{D}. \quad (1)$$

The dielectric displacement \mathbf{D} is given as

$$\mathbf{D} = \epsilon_0 \epsilon \mathbf{E} + \mathbf{P}_{fl} \quad (2)$$

and the dielectric tensor ϵ and the conductivity tensor $\boldsymbol{\sigma}$ read as

$$\epsilon_{ij} = \epsilon_{\perp} \delta_{ij} + \epsilon_a n_i n_j, \quad \sigma_{ij} = \sigma_{\perp} \delta_{ij} + \sigma_a n_i n_j. \quad (3)$$

The flexo polarization \mathbf{P}_{fl} , which is finite in the presence of spatial variations of \mathbf{n} , is defined as follows [3, 4, 16]

$$\mathbf{P}_{fl} = e_1 \mathbf{n} (\nabla \cdot \mathbf{n}) + e_3 (\mathbf{n} \cdot \nabla) \mathbf{n} \quad (4)$$

with the flexo coefficients e_1, e_3 . Because of $\text{curl } \mathbf{E} = 0$ it is convenient to rewrite Eq. (1) in terms of the electric potential, Φ . The resulting equation contains in its linearized version only the sum ($e_1 + e_3$) of the flexo coefficients [see Eq. (A.11)]. The flexo polarization contributes also to the electric torque on the director, but for EC this is of minor importance. Here the parameter combination ($e_1 - e_3$) comes into play [see Eqs. (A.6) and (A.7)]. Note that the so called dynamic flexoelectric effect [5] does not contribute to the linearized nematohydrodynamic equations.

It is convenient to parameterize the strength E_0 of the applied electric ac field or the rms value U of the applied voltage, respectively, in terms of the dimensionless control parameter R :

$$R = \frac{\epsilon_0 E_0^2 d^2}{k_0 \pi^2} \equiv \frac{\epsilon_0 2U^2}{k_0 \pi^2}, \quad (5)$$

with ϵ_0 the permittivity of the free space and $k_0 = 10^{-12} N$ a measure of elastic constants in the orientational free energy. Convection sets in at the threshold voltage, U_c , which depends on the material constants of the specific nematic. U_c increases monotonously with increasing frequency f and varies usually between 5 V and 100 V.

The linear system of PDE's for the perturbations of the electric potential ϕ , for the director distortions n_y, n_z and the velocity field \mathbf{v} in \mathbf{q} -space [see Eq. (A.5)] can be written in the symbolic form

$$\mathcal{C} \frac{\partial}{\partial t} \mathbf{V}(\mathbf{q}, z, t) = \mathcal{L}(R) \mathbf{V}(\mathbf{q}, z, t), \quad (6)$$

where we introduced the symbolic vector $\mathbf{V}(\mathbf{q}, z, t) = (\phi, n_z, n_y, \mathbf{v})$. The operators \mathcal{C} and $\mathcal{L}(R)$, which can be read off from Eqs. (A.6)–(A.11), are combinations of linear differential operators in z with coefficients, that are periodic in time with circular frequency $\omega = 2\pi f$ and which depend on the wave vector $\mathbf{q} = (q, p)$ as well. For normal rolls with \mathbf{q} parallel to \mathbf{n}_0 [i.e., $\mathbf{q} = (q, 0)$] the fields n_y and v_y vanish identically.

In view of time periodicity Eq. (6) is solved with a Floquet ansatz in time

$$\mathbf{V}(\mathbf{q}, z, t) = \text{Re} \left(\exp[\sigma(\mathbf{q})t] \mathbf{V}_{lin}(\mathbf{q}, z, t) \right) \quad (7)$$

with $\mathbf{V}_{lin}(\mathbf{q}, z, t) = \mathbf{V}_{lin}(\mathbf{q}, z, t + 2\pi/\omega)$. Thus we arrive from Eq. (6) at the linear eigenvalue problem

$$\sigma(\mathbf{q}, R) \mathcal{C} \mathbf{V}_{lin}(\mathbf{q}, z, t) = (\mathcal{L} - \mathcal{C} \frac{\partial}{\partial t}) \mathbf{V}_{lin}(\mathbf{q}, z, t). \quad (8)$$

We are interested in the growth rate, $\sigma_0(\mathbf{q}, R)$, i.e., in the eigenvalue $\sigma(\mathbf{q}, R)$ with the largest real part. The condition $\text{Re}[\sigma_0(\mathbf{q}, R)] = 0$ yields the neutral surface $R = S_0(\mathbf{q})$ with its minimum $R_c = S_0(\mathbf{q}_c)$ at the critical wave vector \mathbf{q}_c . If the imaginary part of $\sigma_0(\mathbf{q}, R)$ vanishes simultaneously with its real part at $\mathbf{q} = \mathbf{q}_c$ and $R = R_c$, the bifurcation is stationary; otherwise we speak of an

oscillatory (Hopf) bifurcation. In fact oscillatory bifurcations to EC have not been found in the present linear eigenvalue problem.

The boundary conditions for $\mathbf{V}_{lin}(z, t)$ (we will suppress the \mathbf{q} -dependence in the following) with respect to z at $z = \pm d/2$ (see Appendix) are automatically ensured by a Galerkin method: the fields are expanded into complete sets of functions, which vanish at the boundaries. Similarly, the periodicity in time of \mathbf{V}_{lin} is guaranteed using (truncated) Fourier expansions in time. For instance, the ansatz for the director component $n_z(z, t)$ of $\mathbf{V}_{lin}(z, t)$ reads as follows

$$n_z(z, t) = \sum_{n=1}^N \sum_{k=-K}^K \bar{n}_z(n|k) \exp[i k \omega t] S_n(z), \quad (9)$$

with $S_n(z) = \sin[n\pi(z/d + 1/2)]$ and $\bar{n}_z(n|k)^* = \bar{n}_z(n|k)$. An analogous ansatz is used for the corresponding Fourier amplitudes ϕ, n_y, v_x, v_y as defined in Eq. (A.5), whereas for v_z Chandrasekhar functions [6, 21] replace the S_n . Note that the terms with odd indices $n = 1, 3, \dots$ are symmetric with respect to the reflection $z \rightarrow -z$ at the midplane $z = 0$, whereas those with even $n = 2, 4, \dots$ are antisymmetric. Thus we arrive from Eq. (8) at a linear algebraic eigenvalue problem to determine $\sigma_0(\mathbf{q}, R)$ and the corresponding expansion coefficients $\bar{n}_z(n|k)$, etc. of the linear eigenvector. The summations as in Eq. (9) have to be truncated. Typically a truncation at $K, N = 10$ is well sufficient to obtain an accuracy of better than 1%. This has been checked by increasing systematically the number of modes and monitoring the changes in the eigenvalues and the eigenvectors.

Inspection of the linear equations in the Appendix shows that the transformation

$$\mathcal{T} : (z, t) \rightarrow (-z, t + \pi/\omega) \quad (10)$$

either reproduces or reverses the sign of the Fourier amplitudes as follows

$$\mathcal{T}(\phi, n_z, n_y, v_x, v_y, v_z) \rightarrow \mathbf{p}(-\phi, n_z, -n_y, -v_x, -v_y, v_z) \quad (11)$$

with the parity $\mathbf{p} = \pm 1$. As a consequence of that symmetry the possible eigenvectors of Eq. (8) fall into two classes. The first one (even parity, $\mathbf{p} = 1$) is characterized by $\bar{n}_z(n|k) = 0$ for even $|k+n|$, while for the second, odd-parity class ($\mathbf{p} = -1$) $\bar{n}_z(n|k) = 0$ holds for odd $|k+n|$. Let us indicate contributions to the fields, which are symmetric against $z \rightarrow -z$ [i.e., with odd indices n in the expansion like Eq. (9)], with the symbol \mathfrak{s} and correspondingly the antisymmetric ones (even n) with the symbol \mathfrak{a} . With respect to time the symbol \mathfrak{o} (\mathfrak{e}) is used to indicate the contributions of Fourier modes with odd (even) indices k . Thus for each variable we have four different combinations of the symbols $\mathfrak{e}, \mathfrak{o}$ and $\mathfrak{s}, \mathfrak{a}$ which we list in the Table I. It is obvious that the combinations

TABLE I: Table of possible symmetries of the field variables.

Type	Φ	n_z	n_y	v_x	v_y	v_z
I	$\sigma\mathfrak{s}$	$\epsilon\mathfrak{s}$	$\epsilon\mathfrak{a}$	$\epsilon\mathfrak{a}$	$\epsilon\mathfrak{a}$	$\epsilon\mathfrak{s}$
II	$\sigma\mathfrak{a}$	$\epsilon\mathfrak{a}$	$\epsilon\mathfrak{s}$	$\epsilon\mathfrak{s}$	$\epsilon\mathfrak{s}$	$\epsilon\mathfrak{a}$
III	$\epsilon\mathfrak{s}$	$\sigma\mathfrak{s}$	$\sigma\mathfrak{a}$	$\sigma\mathfrak{a}$	$\sigma\mathfrak{a}$	$\sigma\mathfrak{s}$
IV	$\epsilon\mathfrak{a}$	$\sigma\mathfrak{a}$	$\sigma\mathfrak{s}$	$\sigma\mathfrak{s}$	$\sigma\mathfrak{s}$	$\sigma\mathfrak{a}$

in the rows I and IV belong to $\mathbf{p} = 1$, while those in the rows II and III are associated with $\mathbf{p} = -1$.

For clarity we present explicitly the leading terms of $n_z(z, t)$ in the expansion Eq. (9) for the different symmetries, where the expansion coefficients are written in terms of their moduli $N_z(n|k)$ and phases $\chi(n|k)$

$$\begin{aligned} \bar{n}_z(n|k) &= N_z(n|k) \exp[i\chi(n|k)], \\ \text{with } N_z(n|-k) &= N_z(n|k). \end{aligned} \quad (12)$$

We obtain thus from Eq. (9) for the Type I solution

$$\begin{aligned} n_z^I(z, t) &= S_1(z) \{N_z(1|0) + N_z(1|2) \cos[2\omega t + \chi(2|2)] \\ &\quad + \dots\} \\ &+ S_3(z) \{N_z(3|0) + N_z(3|2) \cos[2\omega t + \chi(3|2)] \\ &\quad + \dots\} + \dots, \end{aligned} \quad (13)$$

and for the Type III solution

$$\begin{aligned} n_z^{III}(z, t) &= S_1(z) \{N_z(1|1) \cos[\omega t + \chi(1|1)] \\ &\quad + N_z(1|3) \cos[3\omega t + \chi(1|3)] + \dots\} \\ &+ S_3(z) \{N_z(3|1) \cos[\omega t + \chi(3|1)] \\ &\quad + N_z(3|3) \cos[3\omega t + \chi(3|3)] + \dots\} + \dots. \end{aligned} \quad (14)$$

The expansion for Type II solutions is analogous to Eq. (14) except that the even z -modes have to be replaced by the odd ones. In the same manner the expansion of Type IV derives from the expansion of Type I. According to Eq. (A.5) we recover $\delta n_z(\mathbf{x}, z, t)$ in real space by multiplying the expressions given in Eqs. (13), (14) with $\cos(\mathbf{q} \cdot \mathbf{x})$.

We will use in this paper the acronym ‘‘conductive’’ to characterize the even-parity solutions corresponding to a combination of the modes with symmetry Type I and IV. That case is realized in the low frequency ‘‘conductive’’ regime in standard EC. The moduli of the expansion coefficients of Type I are in this case typically much larger than those of Type IV and the coefficient $N_z(1|0)$ is dominant. In the absence of the flexo effect mode IV is even decoupled from mode I and is not relevant for the threshold behavior. Analogously the acronym ‘‘dielectric’’ is used to characterize the odd-parity symmetry class, corresponding to a combination of the solutions of symmetry Type II and III. That pattern is realized at higher frequencies in the so called ‘‘dielectric’’ regime of standard EC. The moduli of the expansion coefficients of Type III are in this case typically much larger than those of Type II and the coefficient $N_z(1|1)$ is dominant.

In the absence of the flexo effect the solution of Type II is decoupled from the Type III one and is not relevant for the threshold behavior. Due to the dominance of the modes with small indices k, n , as in Eqs. (13), (14), the threshold behavior of EC for zero flexo coefficients can be described quite well by analytical ‘‘one-mode’’ formulas by restricting the expansions to the leading modes [1].

III. NONSTANDARD CONVECTION

While electroconvection for positive σ_a is well understood in terms of the Helfrich mechanism, the nonstandard case ($\sigma_a < 0, \epsilon_a < 0$) needs a new analysis. We will in particular demonstrate that for negative σ_a the inclusion of the flexo polarization is crucial.

To elucidate the qualitative features of EC it is useful to concentrate on a representative material parameter set. If not otherwise stated, all results given in this section are based on the material parameters of the widely used nematic 4-methoxybenzylidene-4'-n-butylaniline (MBBA), in particular with respect to the elastic constants k_{ii} and the viscosity coefficients α_i [see Eq. (A.14)]. To reveal the particular influence of σ_a and of the flexo coefficients e_i we have, however, allowed for their systematic variations in our theoretical parameter studies.

At first we present the onset behavior of EC, obtained on the basis of the linear equations presented in the Appendix. In Fig. 1 we show the threshold voltage U_c as a function of the dimensionless circular frequency $\omega\tau_q$ ($\omega = 2\pi f$) for a 40 μm thick cell for different σ_a/σ_\perp , but using otherwise the MBBA parameters Eq. (A.14). The charge relaxation time τ_q is defined in Eq. (A.1) and $\omega\tau_q = 1$ corresponds to a frequency of about 34 Hz. We have not resolved here the regime of very small $\omega\tau_q$ where the theoretical analysis becomes more difficult and which is also typically avoided in experiments. For $\sigma_a/\sigma_\perp = 0.5$ (the MBBA value) we observe in Fig. 1 the standard threshold behavior exhibiting the conductive branch at low frequencies with a crossover to the dielectric branch at $\omega = \omega_c = 2\pi f_c$. Note, that the curvature of the $U_c(\omega)$ curve in the conductive regime is concave in contrast to be convex in the dielectric regime. Reducing σ_a/σ_\perp leads to a shrinking of the conductive regime at the expense of the dielectric one, which covers eventually the whole frequency range for $\sigma_a/\sigma_\perp = 0.05$. Further reduction of σ_a/σ_\perp (passing through zero to negative values) leads to a considerable increase of the critical voltage; at the same time the ω -dependence becomes more and more linear.

Fig. 2 exhibits the absolute value $|\mathbf{q}_c|$ of the critical wave vector $\mathbf{q}_c \equiv (q_c, p_c)$ for the parameters of Fig. 1. For $\sigma_a/\sigma_\perp > 0.05$ we observe a jump of $|\mathbf{q}_c|$ from small values below the crossover frequency ω_c to considerably larger values for $\omega > \omega_c$. Decreasing σ_a/σ_\perp leads to an overall continuous frequency dependence. For negative values of σ_a the $|\mathbf{q}_c|(\omega)$ curve becomes almost flat. Note that the relatively small values of $|\mathbf{q}_c| \approx 4\pi/d$ are com-

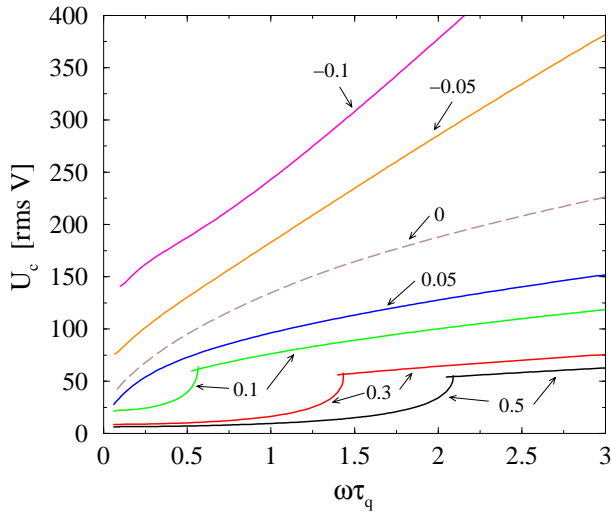


FIG. 1: (Color online) Critical voltage U_c as function of $\omega\tau_q$ for different σ_a/σ_\perp as indicated by the arrows.

parable to values of the standard conductive EC regime, even though the parity of the linear eigenvector [as also indicated by the shape of the $U_c(\omega)$ curves] corresponds to a dielectric mode.

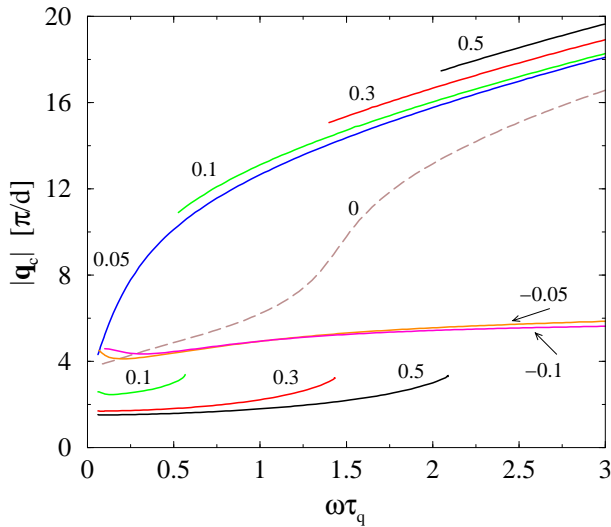


FIG. 2: (Color online) Modulus of the critical wave vector q_c as function of $\omega\tau_q$ for different σ_a/σ_\perp .

Finally, we address the obliqueness angle $\alpha = \arctan(p_c/q_c)$ of the rolls in Fig. 3. For $\sigma_a/\sigma_\perp > 0.05$ we observe jumps from $\alpha = 0$ (normal rolls) to finite α (oblique dielectric rolls) at ω_c . For $\sigma_a/\sigma_\perp = 0.1$ and 0.3 the rolls become oblique again at small ω below the so called Lifshitz frequency. With decreasing σ_a/σ_\perp (below 0.05 and moving into the negative range), the angle α increases monotonically and remains almost constant for all $\omega\tau_q$.

The theoretical results shown in Figs. 1–3 express

clearly the main message of this paper, that the parameter combination $\sigma_a < 0$, $\epsilon_a < 0$ does not necessarily prohibit electroconvection, if the flexo polarization \mathbf{P}_{fl} is taken into account.

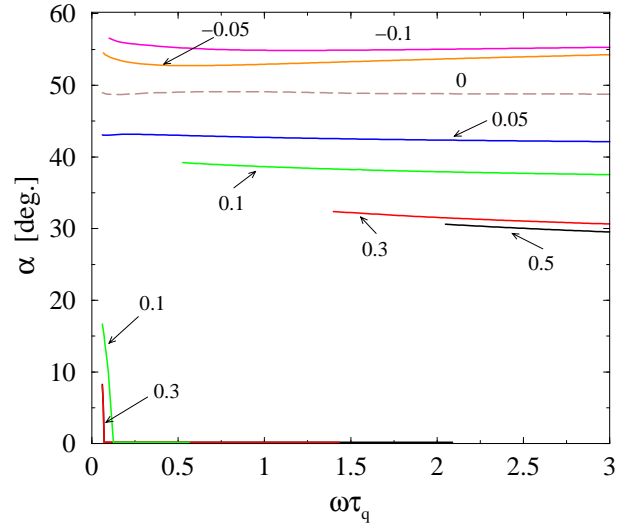


FIG. 3: (Color online) Angle α of the critical wave vector q_c with the x -axis as function of $\omega\tau_q$ for different σ_a/σ_\perp .

To demonstrate that flexo polarization gives rise to a generic mechanism for nonstandard EC ($\sigma_a < 0$) we present the ingredients of the driving positive feedback loop. We make explicitly use of the linear threshold solutions at onset [i.e., at $q_c = (q_c, p_c)$ and $U = U_c$]. It is convenient to rotate the coordinate system in the x - y plane in such a way that the new x -axis (coordinate x') is parallel to q . Thus the centers of the two rolls within one wavelength ($0 \leq x' \leq \lambda_c$) with $\lambda_c = 2\pi/|q_c|$ are located at $x' = 0$ and $\lambda_c/2$, where the director distortion δn_z is maximal at the midplane $z = 0$. At $x' = \lambda_c/4$ and $3\lambda_c/4$, i.e., between the rolls, δn_z vanishes identically.

In Fig. 4 we show the amplitude $n_z(z, t)$ at the midplane $z = 0$ [equal to the director distortion $\delta n_z(x', z, t)$ at the roll center $x' = 0$ according to Eq. (A.5)] as function of time, for one period of the ac voltage. Note that $\delta n_z(x', z, t)$ determines directly the angle between the director and the x - y plane near onset. For definiteness we have fixed in the sequel the undetermined amplitude of the linear eigenvector in such a way, that the maximal value of $n_z = \sin \theta$ corresponds to a tilt angle of $\theta = 10^\circ$. Inspection of Fig. 4 shows that $n_z(0, t)$ can be well represented by a few Fourier modes in time with a small time average. Thus the time variation is obviously dominated by the Type III symmetry (dielectric) solution where the relation $n_z(z, t + \pi/\omega) = -n_z(z, t)$ would hold exactly in the absence of the flexo effect.

In Fig. 5 we present the profile of the amplitude $n_z(z, t)$ for different times as a function of z for $\sigma_a/\sigma_\perp = -0.1$ and $\omega\tau_q = 0.5$. It is obvious that besides the leading mode $\propto \cos(\pi z/d)$ at least the modes $\propto \cos(3\pi z/d)$ and $\cos(5\pi z/d)$ are needed to describe properly the z -

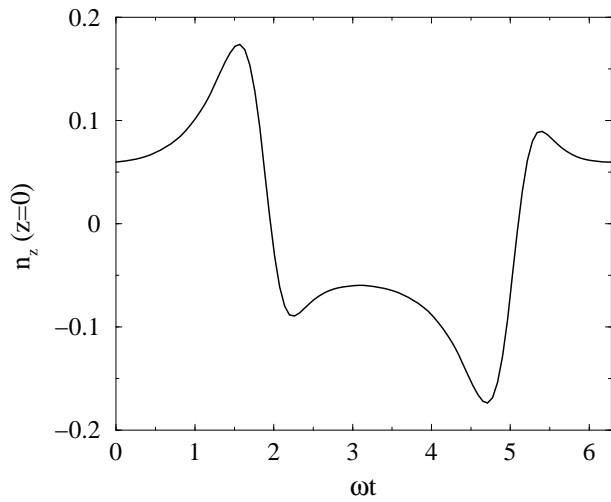


FIG. 4: Temporal evolution of the director amplitude $n_z(0, t)$ for one period $0 < \omega t < 2\pi$ of the driving ac voltage.

dependence.

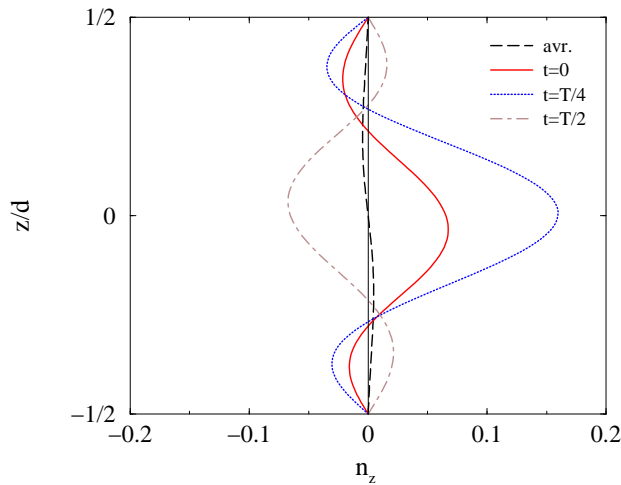


FIG. 5: (Color online) Profile of the amplitude $n_z(z, t)$ along z for different times. The dashed curve marked as “avr.” represents the time average.

The spatial variations of the director field are responsible for the charge separation. In analogy to δn_z Eq. (A.5) the charge density $\rho_{el}(\mathbf{x}, z, t)$ can be represented as the product of $\sin(|\mathbf{q}_c|x')$ and an amplitude $\bar{\rho}_{el}(z, t)$. Thus $|\rho_{el}|$ is maximal between the rolls at $x' = \lambda_c/4, 3\lambda_c/4$. It is useful to single out the flexo contribution, $\rho_{fl} = \nabla \cdot \mathbf{P}_{fl}$, to the total charge density ρ_{el} . In Fig. 6 we present the corresponding amplitude profile $\bar{\rho}_{fl}(z, t)$ which is proportional to $|e_1 + e_3|$. Except near the boundaries $z = \pm d/2$ the flexo charge $\bar{\rho}_{fl}$ has a positive time average with small oscillations superimposed, which is in line with the dominant dielectric symmetry. In Fig. 7 we show the corresponding amplitude $\bar{\rho}_C(z, t)$ of the “Coulomb” charge $\rho_C = \nabla \cdot (\epsilon_0 \epsilon \mathbf{E})$ for the same parameters. It is evident

that $\bar{\rho}_C(z, t)$ is rather small compared to $\bar{\rho}_{fl}$. Since $\bar{\rho}_C$ shows non-symmetric variations in z in addition to strong oscillations in time, the Type II symmetry prevails.

The total charge density $\rho_{el} = \rho_{fl} + \rho_C$ is responsible for the body force $\mathbf{f}_b = \rho_{el} E_0 \cos(\omega t) \hat{\mathbf{z}}$ in the Navier-Stokes equations. For the chosen material parameters, where the main contribution stems obviously from the flexo charge, \mathbf{f}_b oscillates in phase with the driving ac voltage.

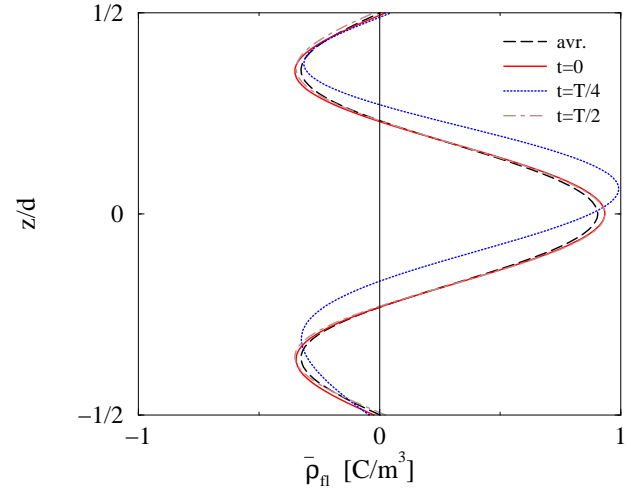


FIG. 6: (Color online) Profile of the amplitude $\bar{\rho}_{fl}(z, t)$ of the flexo charge density along z for different times.

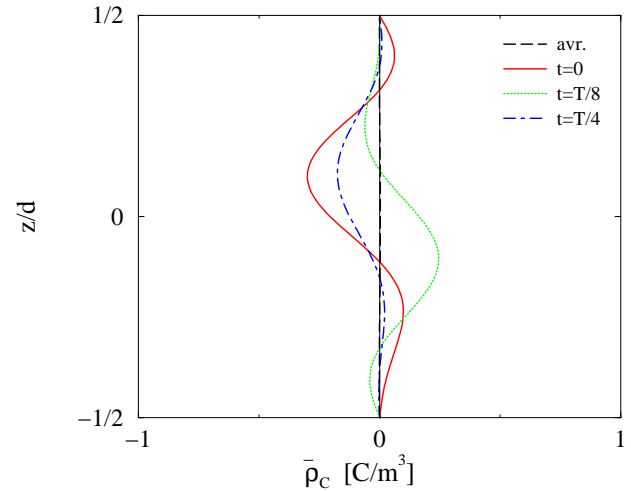


FIG. 7: (Color online) Profile of the amplitude of the Coulomb charge density $\bar{\rho}_C = \bar{\rho}_{el} - \bar{\rho}_{fl}$ along z for different times.

A positive feedback loop to drive EC requires the viscous torque density Γ_y on the director at the roll center to enhance the director fluctuation. According to Eq. (A.6) the director dynamics is governed by the equation

$$\gamma_1 \partial_t n_z(z, t) = [-k_{33} q^2 - k_{22} p^2 + k_{11} \partial_{zz}] n_z(z, t) + \Gamma_y$$

with $\Gamma_y(z, t) = -\alpha_2 q v_z(z, t) - \alpha_3 \partial_z v_x(z, t)$. (15)

The profile of $\Gamma_y(z, t)$ shown in Fig. 8 for different t is calculated with the velocity fields obtained from Eqs. (A.8), (A.9). Near the midplane ($z = 0$) the time dependence can be approximated in leading order as $\Gamma_y(0, t) \propto C \cos(\omega t)$ with $C > 0$. Since the elastic terms $\propto k_{ii}$ are much smaller than the other terms in Eq. (15), the terms $\gamma_1 \partial_t n_z$ and Γ_y have to balance each other. Thus $n_z(0, t) \propto (C/\gamma_1) \sin(\omega t)$ in line with the time dependence in leading order observed in Fig. 4. Therefore the out-of-plane director fluctuations, n_z , and the resulting charge separation, leads to a torque that enhances further the director distortion (positive feedback).

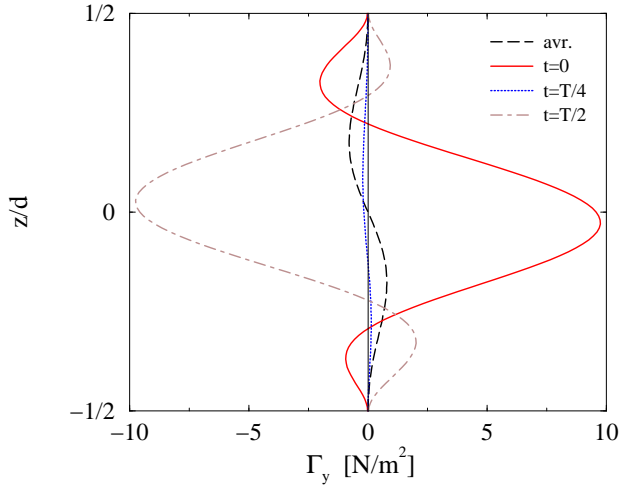


FIG. 8: (Color online) Profile of the torque density $\Gamma_y(z, t)$ on the director along z for different times.

In contrast to ρ_{fl} the Coulomb charge $\rho_C \propto \cos(\omega t)$ does not contribute to the positive feed back loop. It leads to an almost stationary body force \mathbf{f}_b and thus to a torque that is not compatible with the oscillatory director dynamics. Since $\rho_{fl} \propto |e_1 + e_3|$, its contribution to ρ_{el} diminishes with decreasing $|e_1 + e_3|$ and the adverse effect of ρ_C on electroconvection increases. In the limit of $|e_1 + e_3| \rightarrow 0$ we recover the standard model, where ρ_C can be estimated analytically. For the lowest-mode ansatz of dielectric symmetry, $n_z(z, t) = N_z \cos(z) \cos(\omega t)$, the equation for the electric potential ϕ [Eq. (A.11) in Appendix] is easy to solve if $e_i = 0$. Subsequently we obtain from $\rho_{el} = \nabla \cdot \mathbf{D}$ the electric charge density in the form $\rho_{el} \equiv \rho_C = \bar{\rho}_{el}(z, t) \sin(qx + py)$ with

$$\bar{\rho}_{el}(z, t) = \frac{1}{2} \sqrt{Rq} N_z \left(\frac{\sigma_a}{\sigma_{\perp}} - \frac{\epsilon_a}{\epsilon_{\perp}} \right) \times \frac{\epsilon_{\perp}}{1 + \sigma_a q^2 / [\sigma_{\perp} (q^2 + p^2 + 1)]} \cos(z) \quad (16)$$

in dimensionless units. Thus in contrast to $\bar{\rho}_C$ at finite e_i shown above in Fig. 7, $\bar{\rho}_{el}$ presents now a finite time average in line with the Type III symmetry. As soon as $(\sigma_a/\sigma_{\perp} - \epsilon_a/\epsilon_{\perp})$ becomes negative in Eq. (16), the body force \mathbf{f}_b is certainly out-of-phase with the ac driving and the resulting viscous torque is stabilizing, such that EC

is prohibited. For MBBA parameters ($\epsilon_a/\epsilon_{\perp} \approx -0.1$) this would happen for $\sigma_a/\sigma_{\perp} \lesssim -0.1$, i.e., at negative σ_a . The relation $(\sigma_a/\sigma_{\perp} - \epsilon_a/\epsilon_{\perp}) > 0$ is, however, only a necessary condition for the occurrence of EC. In the full linear stability analysis of the standard model ($e_i = 0$) in the dielectric regime the critical voltage diverges in fact already at $\sigma_a/\sigma_{\perp} \approx 0.05$, due to the stabilizing effect of the dielectric torque for $\epsilon_a < 0$. In a similar way it can be shown that for the conductive symmetry [$n_z(z, t) = N_z \cos(z)$] EC excluded for $\sigma_a < 0$, $e_i = 0$ as well. One should mention that for $e_i \neq 0$ a one-mode formula similar to Eq. (16) is not valid due to coupling of modes with different symmetries. Note that for $e_i \neq 0$ an analogous leading-mode approximation becomes more complicated because one needs to take into account at least two modes of the same parity. Moreover, the applicability of such an approximation would be questionable in view of the importance of higher modes in t and z as seen in Figs. 4, 5, respectively.

The eigenvalue problem [Eq. (8)] discussed in the context of EC allows also for a qualitatively different solution family. It is easy to see from Eq. (A.11) that director distortions with a wave vector $\mathbf{q} = (0, p)$ perpendicular to the preferred x -direction do not lead to charge separation. Thus no flow is excited to drive EC. Nevertheless, as first shown by Bobylev and Pikin [17], another kind of pattern forming phase transition remains possible. It arises from the competition between the elastic and the electric contributions to the orientational free energy, if the electric torque $\propto |e_1 - e_3|$ due to the flexo polarization becomes strong enough. In the presence of an ac voltage we find for instance periodic director distortions (flexo domains) $\delta n_z, \delta n_y$ with wavenumber p_{fl} if the dimensionless parameter $\mu = |\epsilon_a k_{11} / (e_1 - e_3)^2| \lesssim 1$. In this situation solutions of both symmetry types, “conductive” as well as “dielectric”, do exist as well.

To study the competition between the flexo domains (depending on $|e_1 - e_3|$) and EC (mainly depending on $|e_1 + e_3|$) we keep the MBBA parameters fixed except $\sigma_a/\sigma_{\perp} = -0.1$ but allow for separate rescaling of the e_i in the form

$$(e_1 - e_3) \rightarrow (e_1 - e_3)\xi_-, \quad (e_1 + e_3) \rightarrow (e_1 + e_3)\xi_+, \quad (17)$$

while so far only the special case $\xi_+ = \xi_- = 1$ has been considered. Since for $\xi_+ = 0$ the flexo charge $\propto |e_1 + e_3|$ becomes zero, EC is impossible for $\sigma_a < 0$.

In Fig. 9 we present the neutral curves in the $U - q$ plane as a function of q at fixed values of p and $\omega\tau_q = 0.5$. Let us start with $\xi_+ = 0$ to block EC, while flexo domains with wave vector $\mathbf{q}_c = (0, p_{fl})$ exist for sufficiently large $|e_1 - e_3|$, i.e., for $\xi_- > 1.4$. The minimum of the neutral curve is at $q = 0$ as demonstrated for $(\xi_-, \xi_+) = (2, 0)$ where $p_{fl} = 4.95\pi/d$. For increasing ξ_+ the flexo charge becomes finite and the curvature of the neutral curve at $q = 0$ decreases and changes eventually sign. In this case the ns-EC minimum develops at $\mathbf{q}_c = (q_c, p_c)$ (oblique rolls). As a representative example we show the neutral curve for $(\xi_-, \xi_+) = (2, 1)$ with its minimum at

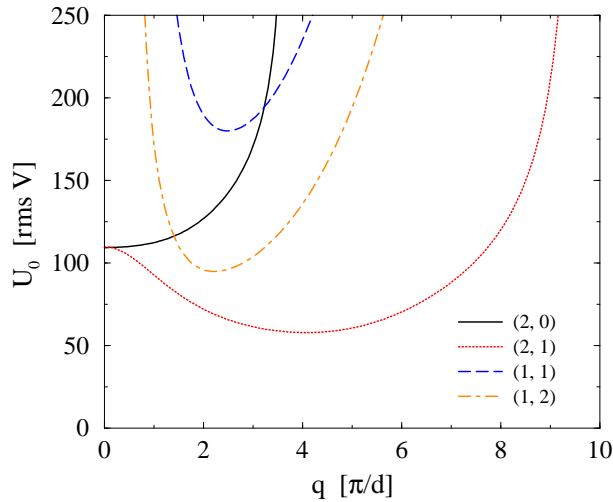


FIG. 9: (Color online) Neutral curves $U_0(q)$ for the wave vector $\mathbf{q} = (q, p)$ as a function of q at a fixed value of p for different magnitudes of the flexo coefficients (ξ_-, ξ_+) at $\omega\tau_q = 0.5$.

$q_c = 4.08\pi/d$ and $p_c = 5.95\pi/d$. In a loose sense the flexo domains have rotated to exploit in addition the flexo charge effect. For comparison we show also two representative curves for $(\xi_-, \xi_+) = (1, 1)$ and $(\xi_-, \xi_+) = (1, 2)$ where the flexo domains do not exist. That is reflected in the divergence of the neutral curves at $q = 0$. With increasing ξ_+ the neutral curve moves down and U_c decreases. Thus, in general, the existence of the flexo domains is a strong indication but not a necessary condition for ns-EC at moderate U_c for $\sigma_a < 0$.

The bifurcation scenarios of ns-EC discussed in this paper cannot be confirmed by experiments with standard MBBA where $\sigma_a > 0$ in the whole nematic temperature range. Fortunately, as already mentioned in the introduction, there are compounds which have $\sigma_a < 0$ at lower T in the nematic phase, while possessing the more common $\sigma_a > 0$ when approaching the nematic-isotropic transition. This sign inversion of $\sigma_a(T)$ is attributed to strong pre-transitional fluctuations due to the existence of a nematic-smectic phase transition at low temperature. In these compounds standard as well as nonstandard EC patterns can be found depending on the temperature. To distinguish these two cases in experiments is not difficult, considering the large angle, α , between \mathbf{q} and \mathbf{n}_0 and the almost linear $U_c(f)$ curve in ns-EC. The observation of the ns-EC patterns requires, however, more experimental efforts because of their lower uniformity and reduced contrast [2, 9, 14, 15].

As a consequence of the strong obliqueness of the rolls the director displays besides the out-of-plane distortions (δn_z) also in-plane rotations (δn_y) which both vanish at the confining plates of the cell. The δn_z distortion is exploited in the conventional shadowgraph technique [22, 23] or in diffraction measurements by shining light on the nematic cell. A finite optical contrast of the pattern requires a finite average of δn_z in the z -direction. Thus

the dielectric modes with symmetry Type III (even in z) play the dominant role. Since they oscillate in time the standard experiments record only certain time averages of the director dynamics. Thus the optical contrast is considerably smaller than in the conductive regime where the director is stationary. In contrast to δn_z the in-plane component δn_y of the director has a large stationary contribution with finite z -average, since in the presence of the flexo effect δn_y is dominated by modes of symmetry Type II. Due to Mauguin's principle in-plane rotations of the director (i.e., of the optical axis) cannot be detected in leading order at small q/k_0 ratios where k_0 denotes the wave number of the incident light. In the next order, however, the local rotation of the optical axis is reflected in depolarization effects, which are typically detected with crossed polarizers. In fact, crossed polarizers turned out to be necessary to detect nonstandard convection in our experiments. This might also explain, why ns-EC in some former experiments without the use of crossed polarizers has not been observed [12].

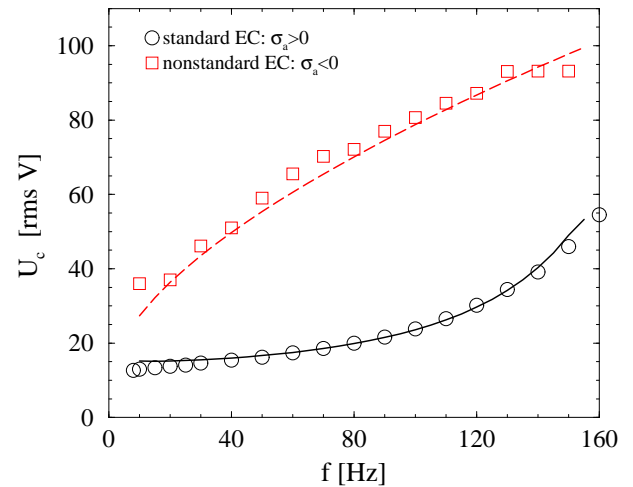


FIG. 10: (Color online) Experimental data (symbols) and theoretical results (lines) for the critical voltage U_c as a function of frequency f for the compound **8/7** for positive as well as for negative σ_a .

As a test of the theoretical predictions new explorative experiments have been carried out on the compound 4-n-octyloxy-phenyl-4-n'-heptyloxy-benzoate (**8/7**, labeled after the number of carbon atoms in the alkyloxy chains). The material showed a nematic order between the nematic-isotropic transition temperature, $T_{NI} = 92^\circ$ and the nematic-smectic C transition temperature, $T_{NS} = 72.5^\circ$. We concentrated on the temperatures close to the T_{NI} where the pre-smectic fluctuations are presumably weaker as in the vicinity of T_{NS} mainly studied before [14, 15]. Figs. 10 and 11 display experimental results on the frequency dependencies of U_c and $|q_c|$, respectively, for a sample of **8/7** with thickness $d = 40 \mu\text{m}$ at two temperatures: $T = 86^\circ\text{C}$ ($\sigma_a < 0$, squares) and $T = 90^\circ\text{C}$ ($\sigma_a > 0$, circles). The data for $T = 90^\circ$ show the charac-

teristic behavior of standard EC in the conductive regime while those for $T = 86^\circ$ conform to the ns-EC features as discussed before in this paper.

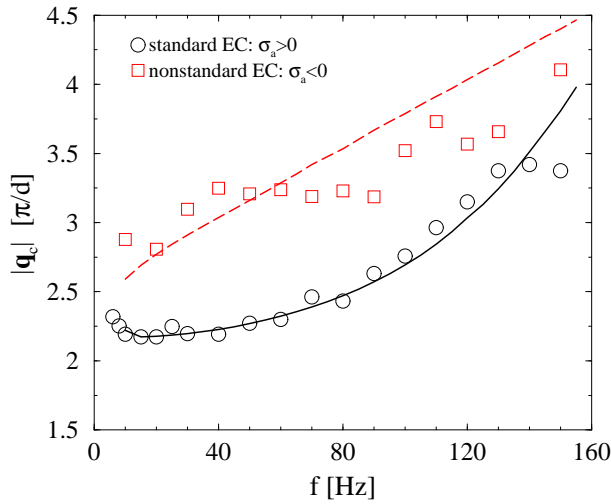


FIG. 11: (Color online) Modulus of the critical wave vector q_c as a function of frequency f for the compound **8/7** for positive as well as for negative σ_a . Experimental data (symbols) and theoretical results (lines).

The solid lines in Figs. 10 and 11 demonstrate that experimental results can be well described by theory. The calculated roll angle α was found to be almost frequency independent and we obtained $\alpha = 0$ for standard and $\alpha = 65^\circ$ for nonstandard EC. This agrees with the experimental values $\alpha = 0$ for standard EC ($T = 90^\circ$) while $\alpha \approx 75^\circ$ for ns-EC ($T = 86^\circ$) is slightly larger than the theoretical value.

In the fitting procedure we have chosen for simplicity the same material parameter set for the nonstandard and standard regime (i.e., for both temperatures $T = 86^\circ\text{C}$ and $T = 90^\circ\text{C}$) except that σ_a was allowed to change. This assumption is supported by the fact that this temperature interval is relatively short within the extended nematic phase; hence one does not expect strong variation of the material parameters except σ_a . Furthermore, viscosities and elastic moduli play a minor role in EC compared to ϵ_a , σ_a and flexo coefficients e_i . The values of ϵ_\perp and ϵ_a were taken from the experiments. The material parameters resulting from fitting [Eq. (A.15)] seem to be realistic. They do not differ too much from the MBBA values (starting point for fitting), except for the considerably large flexo coefficients. In any case these parameters are not claimed to be unique, for instance due to the large scatter in the experimental data of the wave numbers. To reduce the uncertainties in the least square fit one would need in particular measurements of the flexo coefficients e_i .

IV. CONCLUSIONS

The flexoelectric effect, i.e., the occurrence of polarization in a distorted director field, has been described already many years ago [16]. After all, quantitative measurements of this effect and the experimental determination of the flexo coefficients e_1 and e_3 are still difficult. According to earlier theoretical studies of the conductive regime of EC inclusion of the flexo effect does not have an important physical impact [19]. We have repeated those calculations and approved those results.

In contrast, we found that incorporating the flexoelectricity into the standard model is crucial to understand nonstandard EC in the parameter range $\sigma_a < 0$, $\epsilon_a < 0$. Direct quantitative calculations of the threshold and of the critical wave vector have been supplemented by a qualitative analysis of the various mechanisms, which drive EC. We have shown that for $\sigma_a < 0$ without flexoelectricity the charge separation (ρ_C) leads to a stabilizing torque on the director, while including the flexoelectric charge ρ_{fl} the torque yields the favorable conditions for EC. The predictions of the calculations for $U_c(f)$ and $q_c(f)$ confirm the main experimental characteristics of the nonstandard EC patterns observed recently. We have shown that a good agreement could be obtained by a reasonable choice of material parameters for the nematic compound **8/7**.

We mention here that apart from the 4-n-alkoxy-phenyl-4-n'-alkoxy-benzoate homologous series referred to in this paper, patterns now called as ns-EC have also been seen on a few other substances with $\sigma_a < 0$ and $\epsilon_a < 0$ [24, 25]. Several ideas had been suggested as possible explanations like, destabilization of twist fluctuations [24], an isotropic mechanism [25, 26] as well as the flexoelectric effect [20], but no detailed theoretical analysis has been given at that time, especially not in line with the experiments.

Note that recent experimental studies of **8/7** revealed also traveling waves at onset in particular for thinner cells [15]. Hopf bifurcation cannot be captured by the present theory. It is expected that combining flexoelectricity with the weak electrolyte model [27] could give an explanation for traveling ns-EC; this goes, however, beyond the focus of the present paper.

The importance of flexoelectricity in ns-EC is a strong motivation to re-investigate systematically the effect of the flexo polarization also in standard EC. Preliminary theoretical as well as experimental results give the impression that the flexoelectric effect has a stronger influence than assumed so far, in particular in the dielectric regime [28]. Also, the sample thickness appears to be quite important: in particular in very thin (few micron) cells and at low frequencies flexoelectricity has noticeable influence on EC even in the conductive regime [29]. Detailed studies focusing especially on thin samples are in progress.

Finally we would like to remind that the waveform of the applied electric field $\mathbf{E}_0(t)$ influences the onset

behavior of EC. In case of standard EC also subharmonic bifurcations at onset have been found besides the usual ones of conductive or dielectric symmetry [30]. According to theory a subharmonic bifurcation requires that the condition $\mathbf{E}_0(t) = -\mathbf{E}_0(t + \pi/\omega)$ considered in this paper, is not valid. It would be attractive to study the influence of the waveform of driving electric field on nonstandard EC as well.

Acknowledgments

The authors are grateful to G. Pelzl for providing the 8/7 liquid crystal. Financial support by the Deutsche Forschungsgemeinschaft Grant No. Kr690/22-1 and the Hungarian Research Fund OTKA-K61075 are gratefully acknowledged.

APPENDIX: THE LINEARIZED EQUATIONS

Our starting point is a nematic layer of thickness d confined between two parallel plates at $z = \pm d/2$ with the undistorted director $\mathbf{n}_0 = (1, 0, 0)$ in the x -direction and in the absence of flow ($\mathbf{v}_0 = 0$). An ac electric field $\mathbf{E}_0(t) = E_0 \cos(\omega t) \hat{\mathbf{z}}$ is applied in the z -direction between the plates which corresponds to the potential $\Phi_0 = E_0 z \cos(\omega t) = \sqrt{2}U(z/d) \cos(\omega t)$, with $U = E_0 d / \sqrt{2}$ the rms value of applied voltage. According to Eq. (3), the electric properties of the uniaxial nematics are described by the two permittivities, ϵ_{\parallel} and ϵ_{\perp} , and the two conductivities, σ_{\parallel} and σ_{\perp} , parallel and perpendicular to the director, respectively. If the flexo polarization is considered in addition the two flexo coefficients e_1 and e_3 come into play. The orientational elasticity of the director is governed by three constants $k_{ii}, i = 1, 2, 3$, which describe the restoring forces to splay, twist and bend distortions. The viscous contributions to the director and flow dynamics is described by six viscosity coefficients $\alpha_i, i = 1, \dots, 6$ which are not all independent because of the Parodi relation $\alpha_2 + \alpha_3 = \alpha_6 - \alpha_5$.

Inspection of the linear equations shows, that besides the external ac period $2\pi/\omega$ three additional time scales, namely the *charge relaxation time* τ_q , the *director relaxation time* τ_d and the *viscous relaxation time* τ_{visc} govern the dynamics of the linear modes. They are defined as follows:

$$\tau_d = \frac{\gamma_1 d^2}{k_{11}}, \quad \tau_q = \frac{\epsilon_0 \epsilon_{\perp}}{\sigma_{\perp}}, \quad \tau_{visc} = \frac{\rho_m d^2}{\alpha_4 / 2}, \quad (\text{A.1})$$

where $\gamma_1 = \alpha_3 - \alpha_2$ and $\rho_m \approx 10^3 \text{ kg/m}^3$ denotes the mass density of the nematic. The first one is usually the longest, while the third one is the shortest ($\tau_d \sim 20 \text{ s}$ and

$\tau_{visc} \sim 4 \times 10^{-5} \text{ s}$, respectively for a cell of $40 \mu\text{m}$). Thus it is not surprising that inertial effects usually turn out to be negligible. Note that $\tau_q \sim 4 \times 10^{-3} \text{ s}$ is independent on the cell thickness.

The stability of the basic state is studied by the familiar linear stability analysis. Infinitesimal perturbations are superimposed to the basic configuration:

$$\mathbf{n} = \mathbf{n}_0 + \delta\mathbf{n}, \quad \mathbf{v} = \mathbf{v}_0 + \delta\mathbf{v}, \quad \Phi = \Phi_0 + \delta\Phi. \quad (\text{A.2})$$

In leading order in the perturbations one arrives at the linearized nematohydrodynamic equations in the form of linear coupled PDE's in $\delta\mathbf{n}, \delta\mathbf{v}, \delta\Phi$. The instability of the basic state is signaled by the existence of solutions of this linear system that grow exponentially in time.

In this paper we will nondimensionalize the material parameters as follows:

$$\begin{aligned} \alpha_i &= \alpha'_i \alpha_0, \quad k_{ii} = k'_{ii} k_0, \quad \rho_m = \rho'_m \frac{\alpha_0^2}{k_0}, \\ (\sigma_{\parallel}, \sigma_{\perp}) &= (\sigma'_{\parallel}, \sigma'_{\perp}) \sigma_0, \\ (e_1, e_3) &= (e'_1, e'_3) \sqrt{\epsilon_0 k_0}, \end{aligned} \quad (\text{A.3})$$

with

$$\begin{aligned} k_0 &= 10^{-12} \text{ N}, \quad \alpha_0 = 10^{-3} \text{ Pa s}, \\ \sigma_0 &= 10^{-8} (\Omega \text{ m})^{-1}, \quad \epsilon_0 = 8.8542 \times 10^{-12} \frac{\text{A s}}{\text{V m}}. \end{aligned} \quad (\text{A.4})$$

From the director normalization $\mathbf{n}^2 = 1$ it follows immediately that in linear order the possible director distortions are perpendicular to \mathbf{n}_0 , i.e., we use the ansatz: $\delta\mathbf{n} = (0, \delta n_y, \delta n_z)$. Furthermore it is convenient to apply the *curl* to the Navier-Stokes equation to eliminate the pressure. Due to translational invariance in the $x - y$ plane the dependence of the linear solutions on x, y can be separated out in Fourier space. According to [6] the following ansatz is appropriate for that purpose

$$\begin{aligned} \delta\Phi &= \phi(z, t) \sin(qx + py), \\ \delta n_z &= n_z(z, t) \cos(qx + py), \\ \delta n_y &= n_y(z, t) \sin(qx + py), \\ \{\delta v_x, \delta v_y\} &= \{v_x(z, t), v_y(z, t)\} \cos(qx + py), \\ \delta v_z &= v_z(z, t) \sin(qx + py). \end{aligned} \quad (\text{A.5})$$

The equations become nondimensional if lengths are measured in units of d/π , time in units of $\alpha_0 d^2 / (k_0 \pi^2)$ and the electric potential in units of $E_0 d$. One arrives thus at the following linear equations for the z, t dependent Fourier amplitudes ($\phi, n_z, n_y, v_x, v_y, v_z$) in Eqs. (A.5). The primes for nondimensional material parameters defined in Eq. (A.3) are suppressed:

Dynamics of n_z :

$$\begin{aligned} \epsilon_a R \cos(\omega t) q \phi + [\gamma_1 \partial_t + k_{33} q^2 + k_{22} p^2 - k_{11} \partial_z^2 - \epsilon_a R \cos^2(\omega t)] n_z - (k_{11} - k_{22}) p \partial_z n_y \\ + \alpha_3 \partial_z v_x + \alpha_2 q v_z - (e_1 + e_3) \sqrt{R} q \partial_z \phi - (e_1 - e_3) \sqrt{R} \cos(\omega t) p n_y = 0, \end{aligned} \quad (\text{A.6})$$

Dynamics of n_y :

$$\begin{aligned} (k_{11} - k_{22}) p \partial_z n_z + [\gamma_1 \partial_t + k_{33} q^2 + k_{11} p^2 - k_{22} \partial_z^2] n_y - \alpha_3 p v_x - \alpha_2 q v_y \\ + (e_1 + e_3) \sqrt{R} q p \phi - (e_1 - e_3) \sqrt{R} \cos(\omega t) p n_z = 0, \end{aligned} \quad (\text{A.7})$$

Dynamics of v_x, v_y :

$$\begin{aligned} -\alpha_3 p \partial_t \partial_z n_z + (\alpha_2 q^2 - \alpha_3 p^2) \partial_t n_y + [\rho_m \partial_t + (\eta_0 - \eta_1 - \alpha_2) q^2 + \eta_2 (p^2 - \partial_z^2)] p v_x \\ - [\rho_m \partial_t + \eta_1 q^2 + (\alpha_3 + \alpha_4 - \eta_2) p^2 - \eta_3 \partial_z^2] q v_y + (\alpha_3 + \eta_3 - \eta_2) q p \partial_z v_z = 0, \end{aligned} \quad (\text{A.8})$$

Dynamics of v_x, v_z :

$$\begin{aligned} R \cos(\omega t) [\epsilon_\perp (q^2 + p^2 - \partial_z^2) + \epsilon_a q^2] q \phi - \epsilon_a R \cos^2(\omega t) q^2 n_z - (e_1 + e_3) \sqrt{R} \cos(\omega t) q^2 (\partial_z n_z + p n_y) \\ - (\alpha_2 q^2 + \alpha_3 \partial_z^2) \partial_t n_z - \alpha_3 p \partial_t \partial_z n_y + [\rho_m \partial_t + (\eta_0 - \eta_1 - \alpha_2) q^2 + \eta_2 (p^2 - \partial_z^2)] \partial_z v_x \\ - (\alpha_3 + \eta_3 - \eta_2) q p \partial_z v_y - [\rho_m \partial_t + \eta_1 q^2 + \eta_3 p^2 - (\alpha_3 + \alpha_4 - \eta_2) \partial_z^2] q v_z = 0, \end{aligned} \quad (\text{A.9})$$

Continuity equation:

$$q v_x + p v_y - \partial_z v_z = 0, \quad (\text{A.10})$$

Electric potential:

$$\begin{aligned} \sqrt{R} [\epsilon_\perp (q^2 + p^2 - \partial_z^2) + \epsilon_a q^2] \partial_t \phi + \sqrt{R} Q [\sigma_\perp (q^2 + p^2 - \partial_z^2) + \sigma_a q^2] \phi \\ - \sqrt{R} [\epsilon_a \partial_t \cos(\omega t) + Q \sigma_a \cos(\omega t)] q n_z - (e_1 + e_3) q \partial_t (\partial_z n_z + p n_y) = 0. \end{aligned} \quad (\text{A.11})$$

The Eqs. (A.6)-(A.11) contain the main control parameter R defined in Eq. (5) and $Q = \alpha_0 d^2 \sigma_0 / (k_0 \pi^2 \epsilon_0)$, which is proportional to the ratio of the director relaxation time τ_d to the charge relaxation time τ_q . The rotational viscosity γ_1 in the director equations and the shear viscosities $\eta_i, i = 0, \dots, 3$ in the velocity equations, which have been introduced by Miesowicz, are defined as

$$\begin{aligned} \gamma_1 &= \alpha_3 - \alpha_2, \\ \eta_0 &= \alpha_1 + \alpha_4 + \alpha_5 + \alpha_6, \\ \eta_1 &= (-\alpha_2 + \alpha_4 + \alpha_5)/2, \\ \eta_2 &= (\alpha_3 + \alpha_4 + \alpha_6)/2, \quad \eta_3 = \alpha_4/2. \end{aligned} \quad (\text{A.12})$$

The applied voltage $E_0 d \cos(\omega t)$ is kept fixed, the director is assumed to be fixed at $z = \pm \pi/2$ ("strong anchoring"), and for the velocity one has realistic no slip boundary conditions:

$$\begin{aligned} \phi(z = \pm \pi/2, t) &= 0, \\ n_z(z = \pm \pi/2, t) &= 0, \quad n_y(z = \pm \pi/2, t) = 0, \\ \{v_x, v_y, v_z\}(z = \pm \pi/2, t) &= 0. \end{aligned} \quad (\text{A.13})$$

We have used in this paper the standard parameter set of MBBA [nondimensional according to Eq. (A.3)]:

$$\epsilon_\perp = 5.25, \quad \epsilon_a = -0.53, \quad \sigma_\perp = 1.0, \quad \sigma_a = 0.5$$

$$\begin{aligned} e_1 &= -3.25, \quad e_3 = -4.59, \\ k_{11} &= 6.66, \quad k_{22} = 4.2, \quad k_{33} = 8.61 \\ \alpha_1 &= -18.1, \quad \alpha_2 = -110.4, \quad \alpha_3 = -1.1, \quad \alpha_4 = 82.6, \\ \alpha_5 &= 77.9, \quad \alpha_6 = -33.6, \quad \rho_m = 1.0 \times 10^{-3}. \end{aligned} \quad (\text{A.14})$$

Typically the electric conductivities of nematics range between $10^{-1} \sigma_0$ and $10 \sigma_0$. According to Eq. (A.1) the charge relaxation time τ_q is inversely proportional to σ_\perp . If the circular frequencies ω are not too small (i.e., larger than τ_d^{-1}) the σ_\perp dependence can be absorbed by presenting the threshold curves in units of $\omega \tau_q$.

The theoretical curves for **8/7** (see Figs. 10, 11) have been obtained with the parameter set [nondimensional according to Eq. (A.3)]:

$$\begin{aligned} \epsilon_\perp &= 4.2, \quad \epsilon_a = -0.2, \quad \sigma_\perp = 4.0, \\ e_1 &= -9.5, \quad e_3 = -10.5, \\ k_{11} &= 5.0, \quad k_{22} = 3.0, \quad k_{33} = 6.0, \\ \alpha_1 &= 5.0, \quad \alpha_2 = -67.5, \quad \alpha_3 = 12.5, \quad \alpha_4 = 30.0, \\ \alpha_5 &= 22.5, \quad \alpha_6 = -32.5, \quad \rho_m = 1.0 \times 10^{-3}, \end{aligned} \quad (\text{A.15})$$

with $\sigma_a = 0.15$ in the standard EC regime and $\sigma_a = -0.3$ in the nonstandard one.

[1] L. Kramer and W. Pesch, in *Pattern Formation in Liquid Crystals*, edited by Á. Buka and L. Kramer (Springer-

Verlag, New York, 1996) pp. 221.

- [2] For a recent review see: Á. Buka, N. Éber, W. Pesch, and L. Kramer, Phys. Rep. **448**, 115 (2007), and references therein.
- [3] P. G. de Gennes and J. Prost, *The Physics of Liquid Crystals* (Clarendon Press, Oxford, 1993).
- [4] S. Chandrasekhar, *Liquid Crystals* (University Press, Cambridge, 1992).
- [5] H. Pleiner and H. R. Brand, in *Pattern Formation in Liquid Crystals*, edited by Á. Buka and L. Kramer (Springer-Verlag, New York, 1996) pp. 15.
- [6] E. Bodenschatz, W. Zimmermann, and L. Kramer, J. Phys. (France) **49**, 1875 (1988).
- [7] E. F. Carr, Mol. Cryst. Liq. Cryst. **7**, 253 (1969).
- [8] W. Helfrich, J. Chem. Phys. **51**, 4092 (1969).
- [9] Á. Buka, N. Éber, W. Pesch, and L. Kramer, in *Self Assembly, Pattern Formation and Growth Phenomena in Nano-Systems*, edited by A. A. Golovin and A.A. Nepomnyaschy (Springer, 2006) pp. 55.
- [10] W. Pesch and U. Behn, in *Evolution of Spontaneous Structures in Dissipative Continuous Systems*, edited by F. H. Busse and S. C. Mueller (Springer, 1998).
- [11] H. Kresse, A. Wiegeleben, and D. Demus, Krist. Tech. **15**, 341 (1980).
- [12] H. R. Brand, C. Fradin, P. L. Finn, W. Pesch, and P. E. Cladis, Phys. Lett. **A235**, 508 (1997).
- [13] H. Riecke and G. D. Granzow, Phys. Rev. Lett. **81**, 333 (1998).
- [14] E. Kochowska, S. Németh, G. Pelzl, and Á. Buka, Phys. Rev. E **70**, 011711 (2004).
- [15] T. Tóth-Katona, A. Cauquil-Vergnes, N. Éber and, Á. Buka, Phys. Rev. E **75**, 066210 (2007).
- [16] R. B. Meyer, Phys. Rev. Lett. **22**, 918 (1969).
- [17] Yu. P. Bobylev and S. A. Pikin, Sov. Phys. JETP **45**, 195 (1977).
- [18] M. I. Barnik, L. M. Blinov, A. N. Trufanov, and B. A. Umanski Sov. Phys. JETP **46**, 1016 (1977); J. Phys. (France) **39**, 417 (1978).
- [19] L. Kramer, E. Bodenschatz, W. Pesch, W. Thom, and W. Zimmermann, Liquid Crystals, **5**, 699 (1989).
- [20] N. V. Madhusudana and V. A. Raghunathan, Mol. Cryst. Liq. Cryst. Lett. **5**, 201 (1988); Liq. Cryst. **5**, 1789 (1989).
- [21] S. Chandrasekhar, *Hydrodynamic and Hydromagnetic Stability* (Dover Publications Inc., New York, 1981).
- [22] S. Rasenat, G. Hartung, B. L. Winkler, and I. Rehberg, Exp. Fluids **7**, 412 (1989).
- [23] S. P. Trainoff and D. Canell, Phys. Fluids **14**, 1340 (2002).
- [24] M. Goscianski and L. Léger, J. Phys. (France) **36**, 231 (1975).
- [25] L. M. Blinov, M. I. Barnik, V. T. Lazareva, and A. N. Trufanov, J. Phys. (France) **40**, 263 (1979).
- [26] M. I. Barnik, L. M. Blinov, S. A. Pikin, and A. N. Trufanov, Sov. Phys. JETP **45**, 396 (1977).
- [27] M. Treiber and L. Kramer, Mol. Cryst. Liq. Cryst. **261**, 311 (1995).
- [28] W. Pesch and A. Krekhov (unpublished).
- [29] T. Tóth-Katona, N. Éber and Á. Buka (unpublished).
- [30] T. John, J. Heuer, and R. Stannarius, Phys. Rev. E **71**, 056307 (2005).